



**USING TIME-RESOLVED PHOTOLUMINESCENCE TO MEASURE THE
EXCITATION AND TEMPERATURE DEPENDENCE OF CARRIER
RELAXATION IN MID-WAVE INFRARED SEMICONDUCTORS**

THESIS

Kevin Cumblidge, Civilian

AFIT/GAP/ENP/04-02

DEPARTMENT OF THE AIR FORCE

AIR UNIVERSITY

AIR FORCE INSTITUTE OF TECHNOLOGY

Wright Patterson Air Force Base, Ohio

APPROVED FOR PUBLIC RELEASE; DISTRIBUTION UNLIMITED

The views expressed in this thesis are those of the author and do not reflect the official policy or position of the United States Air Force, Department of Defense, or the United States Government.

AFIT/GAP/ENP/04-02

USING TIME-RESOLVED PHOTOLUMINESCENCE TO MEASURE THE
EXCITATION AND TEMPERATURE DEPENDENCE OF CARRIER
RELAXATION IN MID-WAVE INFRARED SEMICONDUCTORS

THESIS

Presented to the Faculty
Department of Engineering Physics
Graduate School of Engineering and Management
Air Force Institute of Technology
Air University
Air Education and Training Command
in Partial Fulfillment of the Requirements for the
Degree of Master of Science (Applied Physics)

Kevin Cumblidge, BS
Civilian

June, 2004

APPROVED FOR PUBLIC RELEASE; DISTRIBUTION UNLIMITED

AFIT/GAP/ENP/04-02

USING TIME-RESOLVED PHOTOLUMINESCENCE TO MEASURE THE
EXCITATION AND TEMPERATURE DEPENDENCE OF CARRIER
RELAXATION IN MID-WAVE INFRARED SEMICONDUCTORS

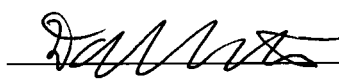
Kevin Cumblidge, BS
Civilian

Approved:



Michael A. Marciniak (Chairman)

4 Jun 04
Date



David E. Weeks (Member)

4 Jun 04
Date



Robert A. Hengehold (Member)

4 Jun '04
Date

Abstract

Research in the field of mid-wave infrared (MWIR) semiconductor photonic devices has led to applications in a variety of disciplines including atmospheric monitoring, optical communications, non-invasive glucose testing for diabetics, and infrared (IR) countermeasures. One of the limiting factors for improving the modulation rates of MWIR devices is the carrier relaxation time. This is the time required for energetic carriers to cool to the edge of their respective bands in a bulk semiconductor material, or to the bottom of a well through inter- and intra-sub-band scattering in a quantum well (QW) structure. From these lower energy states, they can then recombine radiatively in photonic devices. This investigation utilized the nonlinear optical technique of frequency upconversion to perform time-resolved luminescence spectroscopy on epitaxial bulk InAs, InAsSb/InAlAsSb type I QW structure, and InAs/GaInSb type II QW samples to calculate carrier relaxation times in each as a function of excitation irradiance and sample temperature.

This thesis is dedicated to my wife.

Were it not for her insight and encouragement,
I would not have returned to college in the first place.

Acknowledgements

So many things had to happen for me to get to this point in my education. I had the help of too many people to list them individually but I want to offer all of them my sincerest gratitude for their assistance along the way, especially all of my undergraduate physics professors for providing me with a solid foundation in physics. Their enthusiasm and encouragement led me to apply to graduate school.

There are some that I would like to single out, however, for their help above and beyond the call of duty:

I would especially like to thank the The Dayton Area Graduate Studies Institute (DAGSI) for the financial support they provided. I hope to prove to be a good investment by utilizing the education they made possible to the best of my abilities.

I deeply appreciate the counsel and encouragement offered by my advisor, Dr. Michael Marciniak. It was because of his proactive recruitment that I was able to experience the extreme sense of accomplishment that getting this experiment to work brought about.

Were it not for my colleague and friend, Lt. Pete Johnson, I would not have learned nearly as much throughout the whole masters program. His gift of being able to elegantly explain difficult concepts in simple terms helped me over the occasional hurdle and made the whole experience all the more enjoyable. His abilities in the lab were truly a blessing.

Finally, I would like to thank the lab technicians Greg Smith and Mike Ranft for their never-ending help when things went wrong—as all things inevitably do.

Kevin Cumblidge

Table of Contents

	Page
Abstract	iv
Acknowledgements	vi
List of Figures	ix
List of Tables	xi
List of Abbreviations	xii
1. Introduction	1
1.1 Background	2
1.2 Problem Statement	2
1.3 Overview of Results	3
2. Theoretical Background	4
2.1 Electron-Hole Pair Formation and Recombination	4
2.2 Electron Scattering in Semiconductor Materials	5
2.2.1 Electron-Phonon Interaction	6
2.2.2 Hot Phonon Effect	7
2.3 Carrier Cooling in Quantum Wells	7
2.4 Electromagnetic Propagation in Anisotropic Media	8
2.4.1 Dielectric Response to Electric Fields	8
2.4.2 Second Harmonic Generation	9
2.4.3 Sum Frequency Generation	10
2.5 Time-Resolved Photoluminescence	11
2.6 Conditions for Upconversion	13
2.6.1 KTA Bias Cut	15
2.7 Theoretical Background Conclusion	16

	Page
3. Experimental Procedures and Samples	17
3.1 Experimental Setup	17
3.1.1 PL Leg	17
3.1.2 Pump Leg	19
3.1.3 Nonlinear Crystal	19
3.1.4 Sum Frequency Output	20
3.1.5 Time-Averaged Photoluminescence	20
3.2 Experiment Calibration	21
3.3 Sample Description	23
3.4 Experimental Procedures and Samples Conclusion	24
4. Data and Analysis	25
4.1 Analysis Procedure	25
4.2 Intrinsic InAs sample (94-052)	28
4.3 Type I Quantum Well Structure (94-099)	31
4.4 Type II Quantum Well Structure (200-91)	35
4.5 Data and Analysis Conclusion	38
5. Conclusions and Recommendations	39
5.1 Conclusions	39
5.2 Recommendations	39
Appendix A. MatLab Programs	42
A.1 MatLab Program for Fitting Exponential Curve to Rise Time Data	42
A.2 MatLab Program for Plotting a Three-Dimensional Curve of Luminescence Rise Time as a Function of Temperature and Excitation Power	45
Bibliography	47

List of Figures

Figure		Page
1.	Schematic representation of carrier relaxation in a semiconductor. A photon of frequency ν_1 is absorbed creating an electron-hole pair. The electron loses energy by electron-phonon interactions, allowing the electron to cool to the bottom of the conduction band. The electron can then recombine radiatively with an available hole in the valance band producing a reduced energy photon of frequency ν_2	7
2.	Second-harmonic generation (SHG) $\chi^{(2)}$ nonlinear process. (a) Geometry of the interaction. (b) Energy-level description—the intermediate-level and the upper-level are dashed because they represent ‘virtual’ energy levels since they are not energy eigenlevels of the free atom.	10
3.	Sum-frequency generation (SFG) $\chi^{(2)}$ nonlinear process. (a) Geometry of the interaction. (b) Energy-level description.	10
4.	Schematic representation of upconversion mixing at the KTA crystal. The Ti:sapphire pulse arrives at the KTA crystal before the photoluminescence signal (a). As the delay stage continues to move, the Ti:sapphire pulse is convolved with the photoluminescence signal resulting in a sum frequency output (b-f).	12
5.	Phase matching geometry required for upconversion. The pump beam and PL beam enter the crystal at 20° with respect to each other. <i>Adapted from Gorski [8]</i>	14
6.	External geometry of pump, PL, and sum k-vectors.	14
7.	Internal phasematching angle (θ_m) geometry.	16
8.	Optical Table Layout for Time-Resolved Photoluminescence (TRPL)	18
9.	Time averaged photoluminescence for bulk InAs sample	21
10.	Temporal alignment of photoluminescence signal and laser pulse. . .	22
11.	QW structures investigated. (a) Sample 200-91 type II QW structure. (b) Sample 94-099 type I QW structure	24
12.	Example luminescence rise time graph for type II MQW at 77.8K and 250mW excitation power.	26

Figure		Page
13.	Photon counts as a function of time for a type II quantum well structure at an excitation power of 6.25mW and a temperature of 100K.	27
14.	Bulk InAs rise time as a function of excitation power and temperature. Bicubic interpolation was used to smooth data. <i>See appendix A for code.</i>	29
15.	Luminescence rise time of a type I quantum well structure as a function of excitation power at various temperatures.	33
16.	Luminescence rise time of a type I quantum well structure as a function of temperature at various excitation powers.	34
17.	Luminescence rise time of a type II quantum well structure as a function of excitation power at various temperatures.	36

List of Tables

Table		Page
1.	Calculated InAs rise time (psec) as a function of excitation power and temperature. Rise time is measured from the 10%-90% intensity points.	28
2.	Calculated type I quantum well structure rise time (psec) as a function of excitation power and temperature. Rise time is measured from the 10%-90% intensity points.	31
3.	Calculated type II quantum well structure rise time (psec) as a function of excitation power and temperature. Rise time is measured from the 10%-90% intensity points.	35
4.	Calculated rise time (in psec) for type II quantum well sample 200-91 as reported by Gorski [8]. Rise time is measured from the 10%-90% intensity points. Temperature is $77K$	35

List of Abbreviations

Abbreviation		Page
MWIR	mid-wave infrared	iv
IR	infrared	iv
QW	quantum well	iv
SNR	signal-to-noise ratio	3
PL	photoluminescence	4
TRPL	time-resolved photoluminescence	8
SFG	sum frequency generation	8
SHG	second harmonic generation	8
OR	optical rectification	10
DFG	difference frequency generation	11
KTA	potassium titanyle arsenate	13
PRR	pulse repetition rate	17
ZPL	zero path length	21
MQW	multiple quantum well	23
MBE	molecular beam epitaxy	23
ESD	error standard deviation	28

USING TIME-RESOLVED PHOTOLUMINESCENCE TO MEASURE THE EXCITATION AND TEMPERATURE DEPENDENCE OF CARRIER RELAXATION IN MID-WAVE INFRARED SEMICONDUCTORS

1. Introduction

Ever since its invention in 1962, the semiconductor laser has rapidly gained in popularity because of its small size, low cost, and its durable nature. Manufacturing of these devices has grown exponentially since then, driven largely by advances in both communications and data storage technologies. Until recently, the majority of these lasers operated in the visible to near infrared spectrum because it was relatively easy to grow the ternary and quaternary III-V compounds necessary for these devices using GaAs or InP as a substrate. Devices with small enough energy gaps to operate efficiently in the mid-wave infrared (MWIR) spectrum, however, tend to be much more difficult to fabricate due to the lack of suitable lattice-matched substrates.

One area of laser diode technology that is of particular interest to the Air Force is in the field of infrared counter measures—using a laser diode to damage or confound thermal detection devices (i.e. heat-seeking missiles). Since these thermal detection devices operate in the MWIR spectrum that is not absorbed by the atmosphere, the interest is in a device capable of operating somewhere in the $3 - 5\mu m$ range. High temperature operation and high power output are two other criteria of interest. While a laser diode solution would provide the ideal scenario, significant advances have been made in optically-pumped MWIR lasers constructed of antimonide-based quantum structures [3].

One of the limiting factors of materials used in such devices is a parameter known as the carrier relaxation time. This is the time it takes electrons, having been excited high into the conduction band of the semiconductor material, to cool to the band edge through inter- and intra-sub-band scattering. These band-edge carriers are then free to recombine radiatively with available holes in the valance band resulting in luminescence.

This parameter is critical since the overall efficiency of the laser depends heavily on making carriers available for radiative recombination as quickly as possible.

A previous report by Jang *et al.* [9] indicated that most energetic carriers in the conduction band cool to the bandedge within $15 - 25ps$ of excitation. From there, they can recombine with available holes producing photons, thus causing the material to luminesce. As more carriers cool to the bandedge, more radiative recombination occurs producing an increased luminescence intensity. Therefore, a direct correlation between the rise in luminescence intensity and the carrier relaxation over time can be inferred.

1.1 Background

The subject of carrier relaxation time in QW structures has been previously addressed by Boggess *et al.* [3] and Gorski [8] although with differing results. Boggess reported a weak indirect dependence of carrier density on rise time while Gorski found the rise time of the luminescence to increase with carrier density. It has been suggested that one possible cause for this discrepancy could be the total number of excited carriers in each experiment, or the carrier density. At high carrier densities, carriers could impart their energy to phonons which, in turn, could impart their energy back to other carriers, thus increasing the relaxation time. This is known as the hot phonon effect. Since there is a direct relationship between excitation power and carrier density, it should be theoretically possible to observe a minima in luminescence rise times by taking data at excitation powers through the range reported by both Boggess and Gorski. This would correspond to the point where the carrier density is at the necessary threshold for this hot phonon effect to occur.

1.2 Problem Statement

In order to quantify the effects of temperature and excitation level on carrier cooling in MWIR semiconductor materials, time-resolved photoluminescence spectroscopy was employed to measure the luminescence rise times in bulk InAs and quantum well MWIR samples at varying temperatures and excitation levels. Equating the luminescence rise time with carrier cooling time enabled evaluation of the samples for trends as both the

excitation power and sample temperature were varied. The range of excitation powers spanned those previously reported by Boggess and Gorski in order to try to observe an increase in luminescence rise time due to the hot phonon effect.

1.3 Overview of Results

Of the three samples examined, the bulk InAs data provided the most insight into the physics behind carrier cooling as a function of both sample temperature and excitation power. The data clearly exhibited an inverse relationship between sample temperature and photoluminescence rise time. This decrease in rise time with increasing sample temperature plainly demonstrated the temperature dependence of carrier scattering due to ion core vibrations within the crystal lattice. This increased scattering resulted in faster carrier cooling rates. An inverse relationship between excitation power and photoluminescence rise time was also observed and is most likely due to an elevated sample temperature resulting from the irradiance.

The results obtained from the type I and type II QW structures provided no clear trends due to significant variations in the data. These variations were most likely due to experimental error caused by problems inherent with the setup, coupled with a low signal-to-noise ratio (SNR). Even though data was taken at a sampling bin time of 60 seconds to try to minimize the effects of the noise, the lack of intensity of the collected luminescence was still a source of error.

These problems were less pronounced with the InAs sample for two reasons. First, the InAs sample was the strongest MWIR emitter of the three samples studied, resulting in data with the highest SNR. Secondly, the measured rise times for the InAs varied by a factor of approximately 40 throughout the range of excitation powers and sample temperatures. This meant that any variations from run-to-run could be absorbed in the data without any appreciable variation. The QW rise times, however, varied by a factor of two for the type I structure and less than two for the type II structure. As a result, attempts to resolve the discrepancy between the results reported by Boggess [3] and Gorski [8] were inconclusive.

2. Theoretical Background

Since the purpose of this experiment is ultimately to investigate carrier cooling by measuring sample photoluminescence, a brief introduction on the cause of the photoluminescence, the nature of carrier cooling, and the upconversion process is useful.

2.1 Electron-Hole Pair Formation and Recombination

The operation of almost all photonic devices is based on the creation or annihilation of electron-hole pairs. The electron-hole pair formation process involves raising an electron in energy from the valance band to the conduction band, thereby leaving a hole behind in the valance band. These pairs are formed when an energetic particle, incident on a semiconductor, imparts an energy at least equal to the bandgap energy to a valance band electron. One method of creating electron-hole pairs is through photon absorption. For this to occur, photons with an energy greater than the bandgap energy are absorbed and impart their energy to the valence band electrons, thus promoting them into the conduction band.

It is also possible for an electron to loose energy by recombining with an available hole in the valance band. This typically occurs with electrons at the conduction bandedge and can result in a radiative transition where the excess energy is dissipated as photons, usually having energy equal to the bandgap energy given by

$$h\nu = \varepsilon_g \tag{1}$$

where h is Planck's constant, ν is the frequency of the emitted photon, and ε_g is the bandgap energy. These emitted photons are the source of the luminescence measured in this experiment. The process is called photoluminescence (PL) because the electron-hole pairs were created by absorption of photons.

While the preceding discussion was limited to the radiative recombination of electron-hole pairs, it is also possible for electrons and holes to combine through nonradiative transitions. The recombination rate equation that describes how carrier density will change

over time due to spontaneous emission in a semiconductor can be written as [1]

$$-\frac{dn}{dt} = A_{SRH} \cdot n + B_{rad} \cdot n^2 + C_{Auger} \cdot n^3 \quad (2)$$

where n is the carrier density, A_{SRH} is the Shockley-Read-Hall coefficient, B_{rad} is the radiative coefficient, and C_{Auger} is the Auger coefficient. While the nonradiative Shockley-Read-Hall and Auger recombination mechanisms were not considered in this thesis, they have been previously investigated and reported in-depth by other individuals [6, 8, 11].

2.2 Electron Scattering in Semiconductor Materials

In order to introduce the concept of carrier cooling, it is first necessary to discuss the underlying physics behind electron motion in the conduction band. In 1928, Felix Bloch showed quantum mechanically that because of the wave nature of electrons, they can move unimpeded through a perfectly ordered lattice of ions [14]. This implied that electrons in the conduction band of a perfect (infinite) crystal could remain there indefinitely. Grüneisen then used electron transport theory to calculate the scattering probabilities of free electrons migrating in a lattice of ions vibrating according to the Debye theory of lattice heat capacity [5]. He obtained an expression for the temperature dependence of the scattering probability which goes as

$$\frac{1}{\tau_{lat}} \quad (3)$$

where τ_{lat} is the mean time between collisions of electrons with the lattice ions. This does not present the whole picture, however, because it was derived with an assumption of a perfect lattice.

Irregularities in the lattice give rise to a second cause for electron scattering. These include interstitial atoms and impurities, crystal dislocations, and grain boundaries. These irregularities will add to the number of collisions within the crystal lattice per unit time. Since they are properties of the semiconductor sample, however, they are essentially independent of the temperature. The scattering probability is inversely proportional to the mean free time between collisions, so the mean free time between collisions for all contri-

butions to the scattering process can be written as

$$\frac{1}{\tau} = \frac{1}{\tau_{lat}} + \frac{1}{\tau_{imp}} \quad (4)$$

where τ_{imp} is the mean free time between collisions due to all lattice impurities.

In addition to these two carrier-scattering mechanisms, there are other sources of scattering in a real crystal. The process of alloying in semiconductors results in a random positioning of the substituting atom species in the crystal lattice. This causes a perturbation of the periodic potential of the lattice, which manifests itself as an additional scattering mechanism for carriers known as alloy scattering [2]. This scattering process is dominant in alloyed semiconductors.

2.2.1 Electron-Phonon Interaction. As previously stated, it is desirable for electrons, or carriers, at the conduction bandedge to loose energy through radiative recombination. The Pauli exclusion principle, however, introduces the requirement that not all of the electrons can exist simultaneously at the energy level associated with the conduction bandedge. This means that electrons will be distributed in the conduction band of a semiconductor as defined by Fermi-Dirac statistics (assuming thermal equilibrium). The question arises then, as to what happens in a nonequilibrium condition when there are electrons high in the conduction band due to photoluminescence? This is where the concept of carrier cooling enters the picture.

Exciting a semiconductor with a laser pulse creates a nonequilibrium condition, resulting in a carrier temperature higher than the lattice temperature. Initially, carrier-carrier scattering dominates, as energy is exchanged between the carriers created by the pulse. The carrier-carrier scattering quickly dissipates as they reach a common temperature [17]. As time progresses, the process of electron-phonon scattering continues to cool carriers due to the lattice vibrations discussed in section 2.2. In these interactions, the excess energy is imparted to phonons and dissipated as heat in the lattice. Thus, the carriers continue to cool and their temperature eventually approaches the lattice temperature [20]. Electrons already at the bandedge continue to recombine both radiatively and nonradiatively through the processes discussed in equation 2, creating vacant energy levels

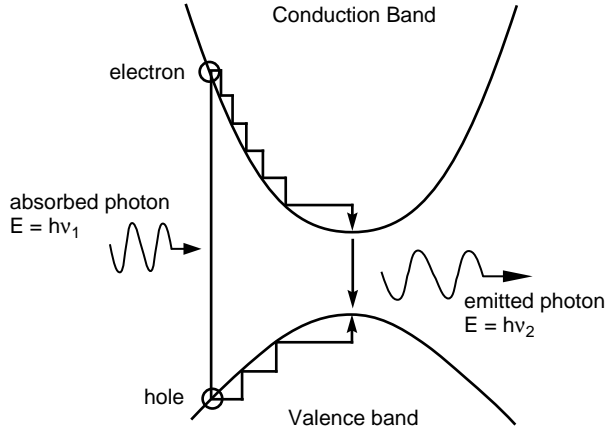


Figure 1 Schematic representation of carrier relaxation in a semiconductor. A photon of frequency ν_1 is absorbed creating an electron-hole pair. The electron loses energy by electron-phonon interactions, allowing the electron to cool to the bottom of the conduction band. The electron can then recombine radiatively with an available hole in the valence band producing a reduced energy photon of frequency ν_2 .

for the cooling carriers. This process is illustrated above in Fig.1, and the end result is that the evolution of the carrier temperature in a semiconductor is closely tied to the rise in the luminescence signal.

2.2.2 Hot Phonon Effect. An interesting phenomena that occurs at very high excitation powers is known as the hot phonon effect. At high carrier densities, a nonequilibrium phonon population arises as carrier cooling creates phonons faster than the phonon energy can be dispersed, creating hot phonons [17]. Energy imparted to phonons from electrons could, in turn, be imparted back to other electrons, thus increasing the relaxation time. This hot phonon effect has been observed and reported by Yang [20].

2.3 Carrier Cooling in Quantum Wells

The previous discussion involved the general (and simplest) case, involving a bulk semiconductor. Photoluminescence, however can also be measured in QW structures. In quantum wells, the electron-hole population is generally created in the barriers, from which they diffuse and thermalize to the lowest bound states in the well region. From there, they are able to recombine radiatively as previously described.

There are significant differences that arise with carrier cooling in QW structures, however. It has been previously reported by Davis that the probability of a transition between discrete electron levels in a quantum well is much smaller than the probability of making a transition in bulk semiconductor due to energy and momentum conservation requirements. This results in a bottleneck of carriers in the bulk-like barrier region to the confined quantum well states as they waited for the transition to the bottom of the well to occur. This bottleneck effect was significantly more pronounced with narrowing well widths. The narrower the well, the less likely the transition will occur, and an increase in carrier relaxation time was observed [7].

2.4 Electromagnetic Propagation in Anisotropic Media

The discussion and diagrams for this section are adapted from Boyd [4] and Schepler [15].

The process of Time Resolved Photoluminescence (TRPL) spectroscopy, as performed in this experiment, is made possible by making use of the nonlinear response of anisotropic materials to electromagnetic propagation. The nonlinear processes utilized in this experiment were sum frequency generation, also known as upconversion, and second harmonic generation or frequency doubling.

In the case of sum frequency generation (SFG), two photons with different frequencies are mixed in an anisotropic media, e.g., a nonlinear crystal, and a photon with a frequency equal to the sum of the two original photons is output. This process is used to time-resolve the photoluminescence from the samples. Second harmonic generation (SHG) is just a special case of SFG where the two input frequencies are equal. SHG was used in the calibration process for this experiment. The following discussion has been provided in order to provide the reader with further insight into the cause of these nonlinear effects.

2.4.1 Dielectric Response to Electric Fields. The dielectric response of a medium to an electric field can be described as an induced polarization (dipole moment per unit volume) as given by

$$D = \epsilon_0 E + P \tag{5}$$

where D is the electric displacement vector, E is the electric field vector ϵ_0 is the permittivity of vacuum, and P is the polarization vector which, as a function of time, can be written as

$$P(t) = \chi^{(1)} E(t) \quad (6)$$

Here, the polarization has been described as a linear response of $\chi^{(1)}$ which is a second-order tensor called the electric susceptibility tensor. In a real atomic system, however, polarization is proportional to the electric field only for small field strengths. For higher field strengths, e.g. those made possible with lasers, the polarizability can be expressed as a Taylor series expansion

$$P(t) = \chi^{(1)} E(t) + \chi^{(2)} E^2(t) + \chi^{(3)} E^3(t) + \dots \quad (7)$$

In this case, the squaring or cubing the E-field can introduce additional frequencies for $P(t)$ where $P(t)$ acts as a driving term for the wave equation given by

$$\nabla^2 E - \frac{n^2}{c^2} \frac{\partial^2 E}{\partial t^2} = \underbrace{\frac{4\pi}{c^2} \frac{\partial^2 P}{\partial t^2}}_{\text{driving term}} \quad (8)$$

The nonlinear processes associated with the second-order $\chi^{(2)}$ term in equation 7 include phenomena such as second harmonic generation, sum frequency generation, and difference frequency generation. The third-order $\chi^{(3)}$ nonlinear processes are responsible for third-harmonic generation and self focusing, also known as the Kerr lens effect. This effect is utilized in a technique known as passive mode locking in the Coherent Ti:sapphire laser used in this experiment, thus enabling the laser to produce a pulsed output.

2.4.2 Second Harmonic Generation. The first experiment in nonlinear optics was performed by Franken, Hill, Peters, and Weinreich in 1961 [21]. It involved the frequency doubling, also known as second harmonic generation (SHG), of a ruby laser pulse in a quartz plate. This concept is illustrated in Fig.2.

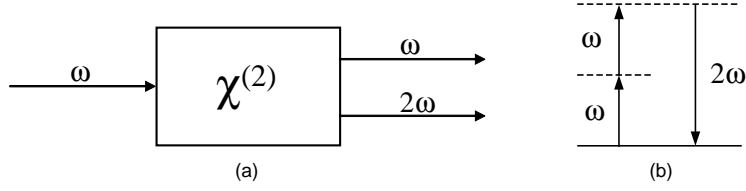


Figure 2 Second-harmonic generation (SHG) $\chi^{(2)}$ nonlinear process. (a) Geometry of the interaction. (b) Energy-level description—the intermediate-level and the upper-level are dashed because they represent ‘virtual’ energy levels since they are not energy eigenlevels of the free atom.

Starting with a plane wave at frequency ω

$$E(t) = Ee^{-i\omega t} \quad (9)$$

The second-order polarization is given by

$$P^{(2)}(t) = \chi^{(2)} E^2(t) = 2\chi^{(2)} EE^* + \chi^{(2)} E^2 e^{-2i\omega t} \quad (10)$$

where the first term on the right is the optical rectification (OR) term and the second term is the wave at frequency 2ω . This basically means that electromagnetic waves of frequency ω with sufficiently large field strength can combine in the nonlinear crystal resulting in an electromagnetic wave of frequency 2ω .

2.4.3 Sum Frequency Generation. Now, consider an optical field made up of two plane waves at frequencies ω_1 and ω_2 incident upon a nonlinear medium as illustrated in Fig.3.

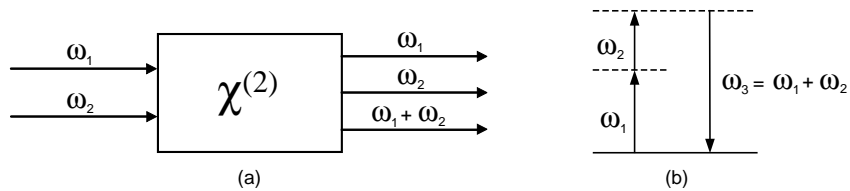


Figure 3 Sum-frequency generation (SFG) $\chi^{(2)}$ nonlinear process. (a) Geometry of the interaction. (b) Energy-level description.

The optical field can be expressed as

$$E(t) = E_1 e^{-i\omega_1 t} + E_2 e^{-i\omega_2 t} \quad (11)$$

and the second-order polarization is given by

$$P^{(2)}(t) = \chi^{(2)} E(t)^2 \quad (12)$$

Inserting the electromagnetic field given by 11 into equation 12 and expanding gives

$$\begin{aligned} P^{(2)}(t) = \chi^{(2)} [& E_1^2 e^{-2i\omega_1 t} + E_2^2 e^{-2i\omega_2 t} + 2E_1 E_2 e^{-i(\omega_1 + \omega_2)t} \\ & + 2E_1 E_2^* e^{-i(\omega_1 - \omega_2)t}] + 2\chi^{(2)} [E_1 E_1^* + E_2 E_2^*] \end{aligned} \quad (13)$$

Note that the first two terms on the right side of equation 13 result in the second-harmonics of ω_1 and ω_2 . The third term gives rise to sum frequency generation (SFG) while the fourth and fifth terms give rise to DFG, or difference frequency generation and OR, respectively.

2.5 Time-Resolved Photoluminescence

While carrier cooling has been previously investigated using a streak camera [7], this experiment utilized a technique known as time-resolved photoluminescence. This was necessary because streak cameras do not work in the IR spectrum. The process of time-resolved photoluminescence was first demonstrated by Mahr and Hirsh [12] and was later described in depth by Shah [16] and is based on the nonlinear optical phenomena known as upconversion.

As previously described in section 2.4.3, upconversion involves the annihilation of two photons in a nonlinear crystal, producing a photon with a frequency equal to the sum of their frequencies. This process only occurs when the incident photons overlap both spatially and temporally. Thus, with the use of ultrafast lasers, one can time-resolve optical signals by mixing them with a short (approximately 140fs) ‘gating pulse’ whose time delay τ can be controlled. As the delay time of the laser pulse is increased the

resultant upconverted signal is a convolution between the emitted luminescence and the laser pulse. This process is illustrated in Fig.4.

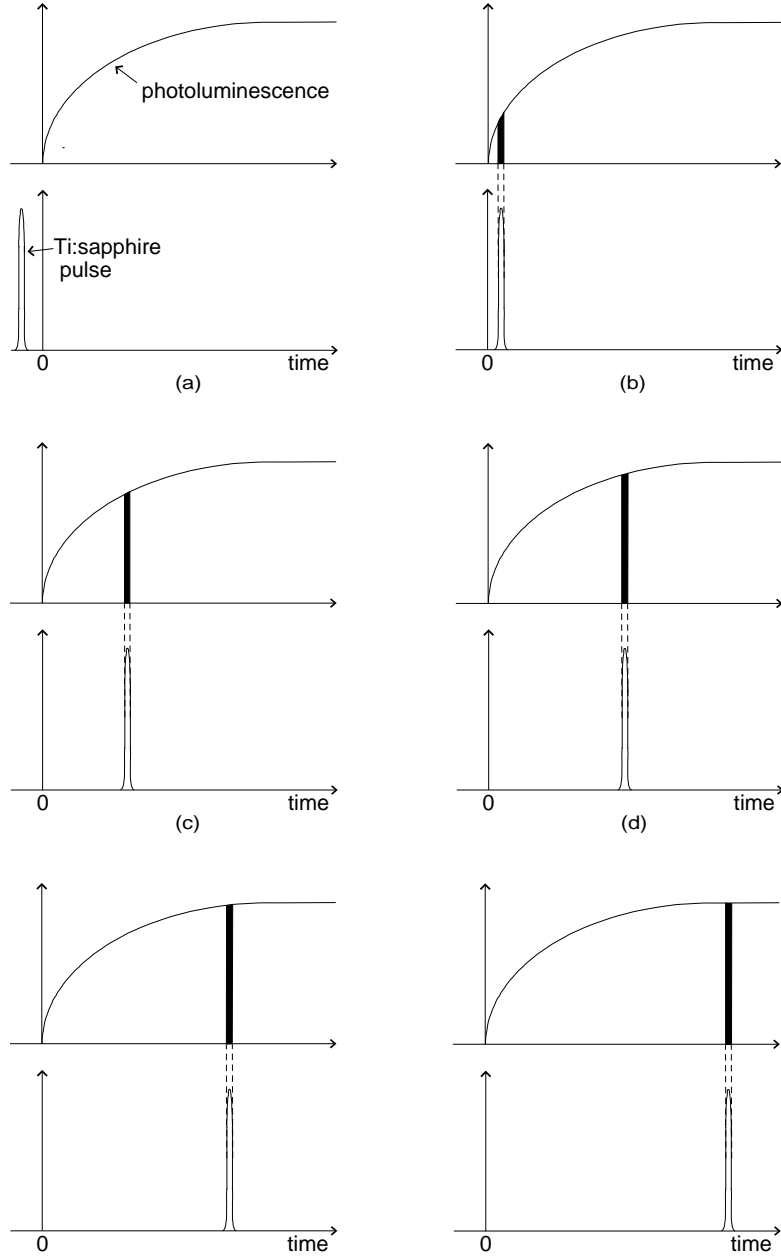


Figure 4 Schematic representation of upconversion mixing at the KTA crystal. The Ti:sapphire pulse arrives at the KTA crystal before the photoluminescence signal (a). As the delay stage continues to move, the Ti:sapphire pulse is convolved with the photoluminescence signal resulting in a sum frequency output (b-f).

The elegance of this method is that the time resolution is comparable to the laser pulse-width enabling one to achieve a resolution on the subpicosecond scale. Since the duration of the PL rise time is on the order of 150 times that of the laser pulse, the laser pulse approximates a Dirac Delta function. As a result, the rise time can be calculated directly from the upconverted signal without having to first deconvolve the data.

2.6 Conditions for Upconversion

In order for upconversion to occur, two conditions must be met. The first is conservation of energy which requires that the sum of the two incoming frequencies equals the sum of the third.

$$\omega_3 = \omega_1 + \omega_2 \quad (14)$$

which in terms of wavelength is given by

$$\frac{1}{\lambda_{Up}} = \frac{1}{\lambda_{PL}} + \frac{1}{\lambda_{Pump}} \quad (15)$$

where λ_{Up} is the upconverted wavelength, λ_{PL} is the MWIR photoluminescence wavelength, and λ_{Pump} is the Ti:sapphire laser wavelength.

The second condition necessary for upconversion is the conservation of momentum, also known as phase matching. This occurs when the momentum vector of the upconverted signal is equal to the sum of the momentum vectors of the PL emission from the sample and the Ti:sapphire pulse.

$$\vec{k}_{up} = \vec{k}_{pl} + \vec{k}_{pump} \quad (16)$$

which is graphically represented in Fig.5.

The indexes of refraction in anisotropic media vary according to the polarization of incoming light and depend on the incident wavelength and angle of incidence. For this experiment, a 1mm thick, 43°-cut biaxial crystal of potassium titanyl arsenate ($KTiOAsO_4$), known as KTA, was used. The KTA crystal was designed for noncollinear, type II, sum-frequency generation using 840nm and MWIR radiation, which is explained below.

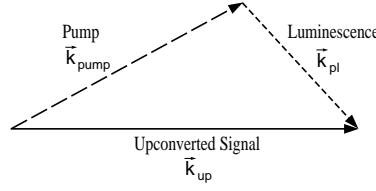


Figure 5 Phase matching geometry required for upconversion. The pump beam and PL beam enter the crystal at 20° with respect to each other. *Adapted from Gorski [8]*

To begin with, the indexes of the KTA crystal can be expressed in terms of the three principal axes, n_x , n_y , n_z which correspond to the index of refraction that would be experienced by a wave polarized along each of the axes. The index of refraction experienced by a wave that is arbitrarily polarized can be calculated from a mathematical model known as an index ellipsoid whose three axes are defined by the magnitudes of n_x , n_y , and n_z .

Type II phase matching refers to the fact that the PL signal is ordinarily polarized, the Ti:sapphire beam is extraordinary polarized, and the resultant upconverted signal is ordinarily polarized. In order to achieve phase matching, the KTA crystal is oriented such that the two incident beams propagate in the x-z plane. Noncollinear mixing means that the MWIR photoluminescence was collected and focused into the KTA crystal while the Ti:sapphire beam was focused onto the same spot on the crystal but at an angle of 20° with respect to the focused luminescence, as is depicted in Fig.6.

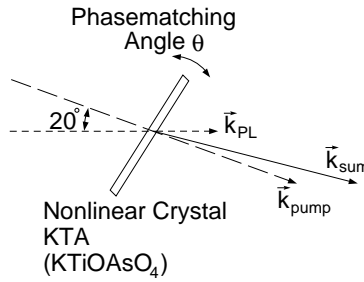


Figure 6 External geometry of pump, PL, and sum k-vectors.

As stated previously, the PL signal is ordinarily polarized. Given the propagation geometry, this means that the PL signal is polarized along the y-axis. Thus, the index of

refraction experienced by the PL signal is given as

$$n_o(\lambda) = n_y(\lambda) \quad (17)$$

where n_o is the index experienced by the ordinary PL signal and n_y is the index of refraction experienced by a wave with the same wavelength as that of the PL signal peak, travelling along the y axis. This value can be calculated using the KTA Sellmeier equation

$$n_y(\lambda) = \sqrt{2.15912 + \frac{1.00099}{1 - (\frac{.21844}{\lambda})^2} - .01096 \cdot \lambda^2} \quad (18)$$

and the index of refraction experienced by the Ti:sapphire beam is given as

$$n_e(\lambda) = \frac{n_x(\lambda)n_z(\lambda)}{\sqrt{n_z(\lambda)^2 \cos(\theta)^2 + n_x(\lambda)^2 \sin(\theta)^2}} \quad (19)$$

where n_e is the index experienced by the extraordinary polarized Ti:sapphire beam and θ is the angle between the propagation vector and the z-axis. The values n_x and n_z are the indexes of refraction experienced by a wave with a wavelength equal to the wavelength of the Ti:sapphire laser travelling along the x and z axes, respectively. They can be calculated using the following KTA Sellmeier equations.

$$n_x(\lambda) = \sqrt{1.90713 + \frac{1.23522}{1 - (\frac{.19692}{\lambda})^2} - .01025 \cdot \lambda^2} \quad (20)$$

$$n_z(\lambda) = \sqrt{2.14786 + \frac{1.29559}{1 - (\frac{.22719}{\lambda})^2} - .01436 \cdot \lambda^2} \quad (21)$$

2.6.1 KTA Bias Cut. There is a problem that can arise when trying to physically realize the theoretical phase matching angle due to Snell's Law. The phase matching angle is measured with respect to the z-axis internal to the crystal as shown in in Fig.7.

The indexes of refraction of the KTA crystal are relatively large at the wavelengths used by this experiment (approximately 1.9) compared to that of air. As a result, it is not always possible to attain the phase matching angle internal to the crystal before the

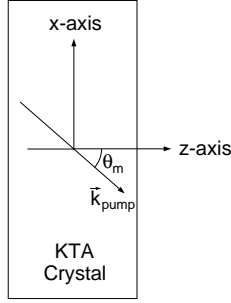


Figure 7 Internal phase-matching angle (θ_m) geometry.

critical angle (the point at which total internal reflection) is reached outside the crystal. This limitation would have manifested itself given the wavelengths used in this experiment. In order to overcome this problem, however, the KTA crystal was pre-cut with a bias so that phase matching was possible. The KTA crystal used in this experiment was cut with a 43° angle from the z-axis, perpendicular to the x-y plane. Thus, upconversion could be accomplished as previously described by tilting the KTA crystal to achieve the correct phase matching angle.

2.7 Theoretical Background Conclusion

This chapter presented the theoretical background necessary to understand the physics behind this experiment. It began with the process of electron-hole pair formation and recombination, explaining carrier creation and how radiative recombination was the source of the PL. The scattering processes that allow excited carriers to cool to the bottom of the conduction bandedge were also described. Next, carrier cooling in quantum wells gave some insight into the differences between carrier cooling in a QW structure as opposed to a bulk sample. From there, a brief overview of electromagnetic propagation in anisotropic media was presented. The chapter concluded with an explanation of TRPL and the conditions necessary to produce upconversion.

Having covered the wide variety of subjects that make up the necessary theoretical background, next the experimental procedures and samples will be examined.

3. Experimental Procedures and Samples

As stated previously, this experiment is based on the process of TRPL. While the theory is relatively straight-forward, its implementation into a physical experiment is fairly complicated. This chapter provides an explanation of the setup and includes a description of the samples that were investigated.

3.1 Experimental Setup

The experimental setup can be seen in Fig.8 and begins at the Coherent Innova 400 Argon-ion (Ar^+) laser. The Ar^+ laser pumps a Coherent Mira 900 mode-locked Ti:sapphire laser operating at $846nm$. The Ti:sapphire laser produces an output beam of $140fs$ pulses at a $76MHz$ pulse repetition rate (PRR) with a total average output power of $2.1W$. The pulse width could be measured by inserting a removable mirror in the path to direct the beam into the APF autocorrelator mounted behind the laser. The autocorrelator would then display the pulse and the width was automatically calculated.

Following the experiment path, the Ti:sapphire beam is expanded, collimated, and then passes through an adjustable half-wave plate before being split into two legs by a polarizing beam splitter. The half-wave plate is used to control the amount of power in each of the legs. The path travelled by the ordinarily polarized beam was used to optically excite the sample and the path it follows will be referred to hereafter as the PL leg. The extraordinary polarized beam was used as the ‘gating’ pulses and its path will be referred to as the pump leg.

3.1.1 PL Leg. The beam travelling down the PL leg begins by passing through a neutral density filter wheel, enabling the power of the excitation beam to be adjusted independently from the beam travelling the pump leg. The beam is then reflected by a corner cube retroreflector to a prism. The retroreflector is mounted to a delay stage so that the optical path length of the PL leg can be varied with respect to that of the pump leg. The prism reflects the beam back to the corner cube which again reflects it back up the bench—this is done to add length to the PL leg. This time the beam misses the prism and is reflected off a mirror where it is then focused onto a semiconductor sample mounted in

a helitran sample chamber, thus causing the sample to luminesce in the MWIR spectrum. The sample chamber is capable of being cooled to a temperature of approximately $5K$ using liquid helium as the cryogen. It is also pumped down to a vacuum level of approximately 10^{-5} Torr in order to prevent condensation from forming on the surface of the sample. Since the sample luminesces in the MWIR spectrum, it is necessary to use a Al_2O_3 (sapphire) window on the chamber due to its low absorption in this frequency range. The sample is mounted on the cold-finger of the helitran such that it is at the focal point of a gold plated off-axis parabolic mirror. This arrangement allows the luminescence from the sample to be reflected and collimated by the parabolic mirror (down the bench) towards another identical off-axis parabolic mirror. The second parabolic mirror focuses the luminescence on a non-linear crystal mounted on a rotational stage. As previously stated in section 2.6, the nonlinear crystal used in the experiment was KTA.

3.1.2 Pump Leg. The beam following the pump leg is directed down the bench where, after being reflected off of three silver mirrors, it is passed through a $700nm$ high-pass filter. It is then reflected once more before passing through a converging lens which focuses it (through a prism) on the KTA crystal. As was described in section 2.5, both beams are focused so that they overlap spatially as well as temporally. For this to occur, the two path lengths have to be identical in length to within $42\mu m$.

3.1.3 Nonlinear Crystal. The choice of a nonlinear crystal is very important. KTA was chosen for this experiment because it possesses the following properties [19]:

1. A large nonlinear optical coefficient—this is the second order tensor $\chi^{(2)}$ given in equation 7 and provides a measure of the upconversion efficiency.
2. A small walk-off angle—this refers to the fact that the crystal is dispersive, meaning that the index of refraction is wavelength dependent. In order to produce upconversion, the two beam paths must overlap inside the crystal. Since the two wavelengths are significantly different, their paths will tend to diverge, or walk-off, due to dispersion.

3. Broad temperature bandwidth—the upconversion efficiency will be relatively independent of temperature variations.
4. Broad spectral bandwidth—this is desirable since there is such a wide difference between the two fundamental wavelengths ($0.846\mu m$ and $3.6\mu m$). Upconversion of this $3.6\mu m$ PL was achievable due to the 43° bias-cut previously discussed in section 2.6.
5. A high damage threshold—using an average pump power of $450mW$ and assuming a top-hat function for the $140psec$ pulses, results in a peak irradiance of approximately $665MW/cm^2$. The crystal needs to be capable of withstanding large electromagnetic fields without being damaged.

3.1.4 Sum Frequency Output. As previously discussed in section 2.4.3, photons of two different frequencies can recombine in a non-linear crystal resulting in a photon with a frequency equal to the sum of the two initial frequencies. Since the sum frequency radiation is significantly weaker but relatively near in frequency to that of the laser, a $700nm$ low-pass filter followed by a $\frac{3}{4}m$ Spex monochromator is used to further reject the unwanted laser signal. The upconverted photons are subsequently detected with a GaAs photomultiplier tube that is configured for photon counting through a computer interface. The weakness of the PL signal coupled with the efficiency of sum-frequency photon generation is such that integration times of up to $60s$ are necessary to obtain as few as 5000 photon counts at the peak of the photoluminescence signal. The delay stage is then incremented via the computer interface and the counting process continues until the all of the data is recorded for the range of interest.

3.1.5 Time-Averaged Photoluminescence. In order to perform TRPL, the monochromator must initially be set to pass the SFG wavelength calculated using equation 15. In order to perform this calculation, however, it is necessary to first determine the peak luminescence wavelength of the sample. This is done by using a procedure known as time-averaged photoluminescence. Referring again to Fig.8, the non-linear crystal is removed from the rotation stage allowing the photoluminescence signal to be collimated and then focused into a Spex 500M $\frac{1}{2}m$ spectrometer. An liquid nitrogen cooled InSb detector is

attached to the spectrometer, which is configured to scan through a programmable range of wavelengths. The detected signal is subsequently plotted on a computer monitor. An example of the time-averaged photoluminescence plot can be seen in Fig.9. The peak luminescence wavelength of the sample can then be easily determined from this plot.

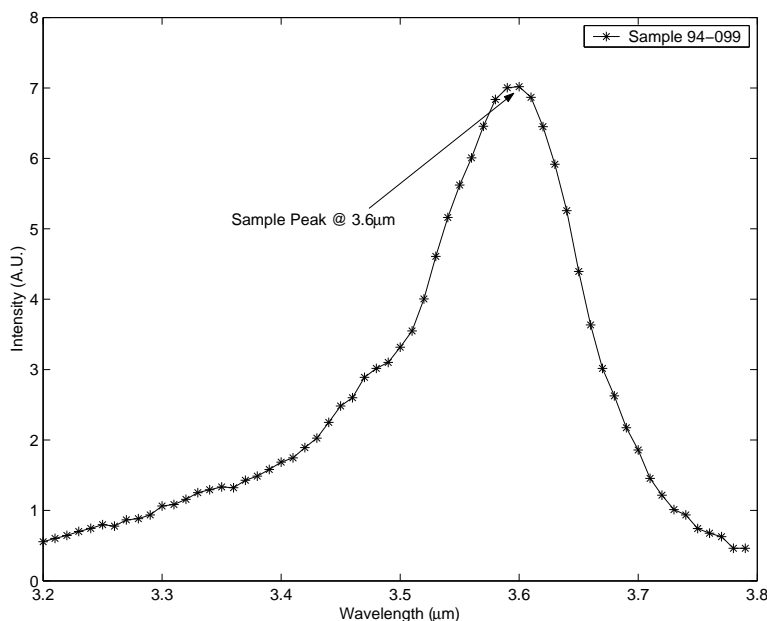


Figure 9 Time averaged photoluminescence for bulk InAs sample

3.2 Experiment Calibration

Two procedures were required to set up the TRPL experiment. First, a general alignment of the table must be performed to ensure all the optics and the sample to be tested are in the correct position. This process has been previously described in great detail by Johnson [11] and as such, will not be reproduced here.

The second alignment is necessary to ensure that the pump pulse and the beginning of photoluminescence signal overlap temporally as seen in Fig.10, thus calibrating the experiment so that the PL rise time can be accurately measured.

This alignment process is known as zero path length (ZPL) since it sets the point where the optical path length of the pump leg is exactly the same as that of the PL

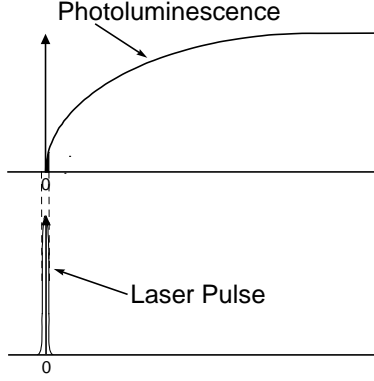


Figure 10 Temporal alignment of photoluminescence signal and laser pulse.

leg. This is easily accomplished by using a $LiIO_3$ crystal to double the frequency of the Ti:sapphire laser utilizing the SHG process described in section 2.4.2.

The alignment begins by mounting a $LiIO_3$ crystal (cut at 39° with respect to the z-axis) to the rotation mount. This pre-cut bias is necessary to physically achieve the internal phase matching angle necessary for SHG as was previously described for the KTA crystal in section 2.6.1. The semiconductor in the sample chamber is then adjusted so that the specular reflection from the PL pulse is being reflected and collimated by the off-axis parabolic mirror. The second parabolic mirror then focuses the specular reflection onto the $LiIO_3$ crystal. The pump pulses follow the pump leg but a $\frac{\lambda}{2}$ wave plate must be inserted in the path in order to change the polarization from extraordinary to ordinary. This is necessary because $LiIO_3$ is a negative uniaxial crystal, meaning that its index of refraction along the ordinary axis n_o is greater than that of the extraordinary n_e axis. In order to achieve SHG, type I ‘ooe’ phasematching is necessary. Type I is a reference to $LiIO_3$ being negative uniaxial and the ‘ooe’ means that two ordinary polarized photons are added and the resultant photon (at double the frequency) is extraordinary polarized.

The $LiIO_3$ crystal is rotated to approximately 16° from perpendicular (with respect to the PL leg) to achieve the necessary phase matching angle. While observing a white screen placed behind the $LiIO_3$ crystal, the delay stage is adjusted until the SHG output is observed as a spot on the screen. Since the Ti:sapphire is operating at $846nm$, the SHG

will be at the visible wavelength of $423nm$. When the experiment is properly calibrated for ZPL, the violet spot is bright enough to be visible under normal lighting conditions.

3.3 Sample Description

Three samples were investigated in this experiment. Sample 94-052 was intrinsic InAs bulk sample of unknown thickness epitaxially grown on an InAs substrate. Using time averaged photoluminescence, it was found to have a peak luminesce at a wavelength of $3.052\mu m$. This sample also had the strongest luminescence emission of all of the samples studied.

Sample 200-91 was a type II multiple quantum well (MQW) structure grown by molecular beam epitaxy (MBE) and had been previously investigated by Gorski for PL rise time [8]. It consists of twenty wells made up of a 20\AA InAs and a 24\AA $\text{Ga}_{0.85}\text{In}_{0.15}\text{Sb}$ layer grown on a GaSb substrate. This structure originally had a GaSb protective cap layer although a reactive ion etch had been used to remove most of this layer. This was necessary to keep the excitation pulse from being absorbed by the GaSb. This sample had a peak luminescence at a wavelength of $3.54\mu m$ with minor peaks at $4.60\mu m$ and $3.30\mu m$. The structure is illustrated in Fig.11(a).

Sample 94-099 was a type I MQW structure grown by MBE on a GaSb substrate. It consists of a total of ten 135\AA wells made up of $\text{InAs}_{0.9117}\text{Sb}_{0.0883}$ surrounded by 321\AA barriers of $\text{In}_{0.88}\text{Al}_{0.12}\text{As}_{0.878}\text{Sb}_{0.122}$. It had a $0.52\mu m$ protective cap layer of $\text{AlAs}_{0.085}\text{Sb}_{0.915}$ which had been previously etched away. Removal of the cap layer from this sample was unnecessary, however, since its bandgap energy is greater than that of the excitation pulse photon energy. Therefore, it would have been transparent to the excitation pulse. The cap layer had originally been removed for research that utilized an excitation pulse frequency of $810nm$, which would have been absorbed by the cap layer.

This sample had a peak luminescence wavelength of $3.60\mu m$ and had the weakest luminescence emission of the three samples. The structure is illustrated in figure 11(b).

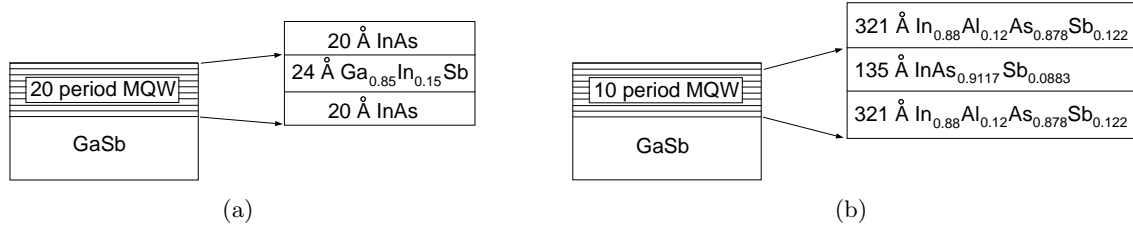


Figure 11 QW structures investigated. (a) Sample 200-91 type II QW structure.
(b) Sample 94-099 type I QW structure

3.4 Experimental Procedures and Samples Conclusion

In this chapter, the experimental setup was presented in detail. The two different optical paths (PL and pump legs) were described, as was the upconverted signal path. The features of the KTA crystal were explained and the convolution process enabling TRPL was depicted. The chapter concluded with an explanation of the experiment calibration followed by a description of the three samples investigated.

Having explained the experimental procedures and samples, it is time to look at the data that was obtained and its analysis.

4. Data and Analysis

At this point, all of the necessary groundwork has been laid. The theory behind the experiment and its physical implementation have been explained. The samples that were investigated have been described. Now it is time to scrutinize the data, beginning with the analysis procedure.

4.1 Analysis Procedure

TRPL was used to record the PL rise for each sample at various excitation levels and various temperatures. The step sizes used were $50ps$ for the bulk InAs and $2ps$ for the QW structures (for reasons that will be explained later). The delay stage was then set to the initial position of five step sizes prior to the point corresponding to ZPL, or time t_0 . This was done in order to take five data points prior to the start of the SFG, enabling the average noise level at time t_0 to be calculated by averaging these points. Ideally, this would give an average background noise count. However, due to long recombination times (greater than $13.2ns$), the luminescence from the sample had not had an opportunity to fully decay before the next excitation pulse had arrived. This means that there were still upconverted photons being counted, as well as background noise counts when the next excitation pulse arrived at the sample. The $13.2ns$ limit was obtained by taking the reciprocal of the Ti:sapphire PRR of $76MHz$.

As stated by Shah [17], the average energy-loss rate per carrier to the lattice is given by

$$\frac{\overline{dE}}{dt} = \frac{-E}{\tau_{3D}} \cdot e^{\frac{-E}{k \cdot T}} \quad (22)$$

where E is the longitudinal optical phonon energy, and T is the carrier temperature and $\frac{1}{\tau_{3D}}$ is the characteristic rate for polar optical phonon scattering and can be treated as a constant for this analysis.

The implication of equation 22 is that since the energy-loss rate is an exponential function (and thus the carrier cooling rate), the rise in luminescence will grow exponentially. The total time for measuring the rise in luminescence signal was varied as necessary for the

luminescence curve to approach its maximum value. This range extended from $50ps$ for the QW structures, up to $1500ps$ for the bulk InAs sample—thus the reason for the different step sizes mentioned previously. The data for each excitation level was then analyzed using the program listed in appendix A, which was used to fit the data to an exponential growth curve of the form

$$U(1 - e^{-\frac{t}{\tau}}) \quad (23)$$

where U is a proportionality constant, t is the time, and τ is the time constant. The values of U and τ are calculated by the program to produce the best fit. The average background (signal+noise at time t_0) was subtracted from the data. The data was then plotted along with the best calculated exponential curve fit. An example of a rise time graph can be seen in Fig.12.

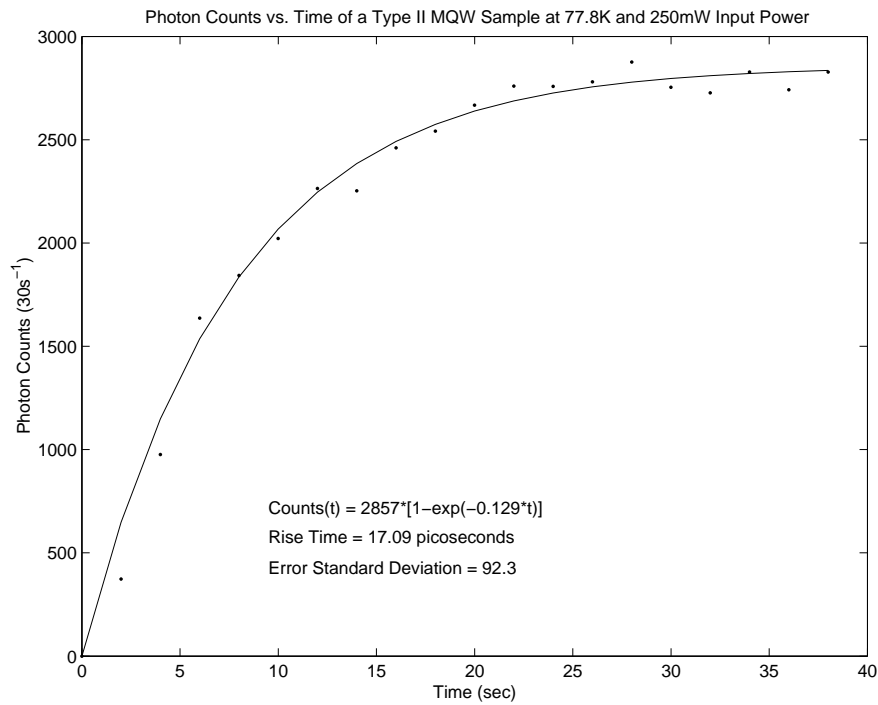


Figure 12 Example luminescence rise time graph for type II MQW at 77.8K and 250mW excitation power.

The expression for the exponential curve, the rise time, and the error standard deviation were also printed on the graph. Further analysis of the data (such as carrier

temperature modelling) was not performed since it required a priori knowledge of carrier density. While previous investigations [13, 8] utilized a technique to map sample luminescence to carrier density, Johnson has reported a possible discrepancy with this method [11].

The rise time was defined as the time necessary for the luminescence intensity to rise from 10% to 90% of its maximum value as determined from the exponential curve fit. This is a standard convention for measuring phenomena with exponential growth and had been used previously by others [7, 8, 18] to compare carrier relaxation times. The 10% and 90% points were determined from the calculated exponential curve because the data taken at the lower excitation powers had enough variation to make accurate determination of these points difficult. This can be clearly seen in Fig.13 (rise times calculated in this fashion are $2.2 \times \tau$).

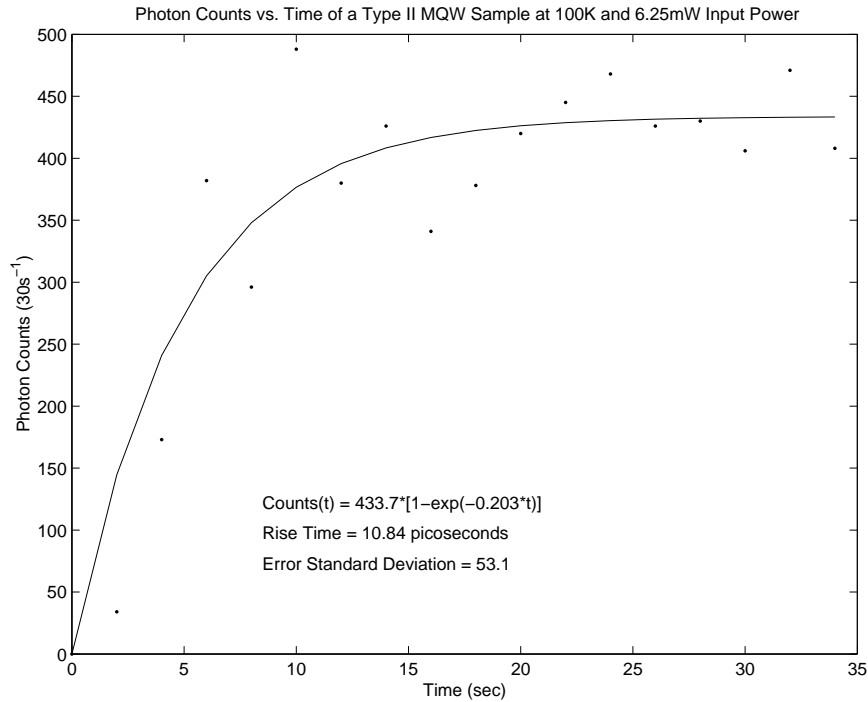


Figure 13 Photon counts as a function of time for a type II quantum well structure at an excitation power of 6.25mW and a temperature of 100K.

The error standard deviation (ESD) was defined as

$$\sqrt{\frac{1}{N} \sum_{i=1}^N (x_i - x_c)^2} \quad (24)$$

where N equals the total number of data points, x_i is the measured data value, and x_c is the calculated exponential fit value. The ESD provides a method whereby the accuracy of the fit can be compared from graph-to-graph. This is easily accomplished by dividing the ESD by the proportionality constant U given in equation 23. The square of the ESD (essentially the variance) was also used in the program to calculate the best value of τ . This was accomplished by finding the value of τ that minimized the variance.

4.2 Intrinsic InAs sample (94-052)

The analysis will begin with the results obtained from the intrinsic InAs sample since they were both the most dramatic and provided the most insight into carrier cooling of the three samples studied. The data is presented below in table 1.

Table 1 Calculated InAs rise time (psec) as a function of excitation power and temperature. Rise time is measured from the 10%-90% intensity points.

Power	100K	78K	35.4K	5.2K
250mW	35.35	58.74	306.5	590.1
200mW	36.85	53.08	302.0	904.7
150mW	40.47	50.59	343.4	1014
100mW	35.40	63.43	454.9	1117
25mW	42.58	66.47	507.1	1412

As previously discussed in section 2.2, carrier cooling occurs as a result of various scattering processes. The mean free time between collisions in a semiconductor material is given by equation 4 where scattering is due to a combination of lattice vibrations and impurities.

Current epitaxial growth techniques enable very pure binary III-V semiconductor materials such as InAs to be produced. This purity leads to carrier cooling predominantly through electron-phonon interactions due to lattice scattering and is clearly illustrated

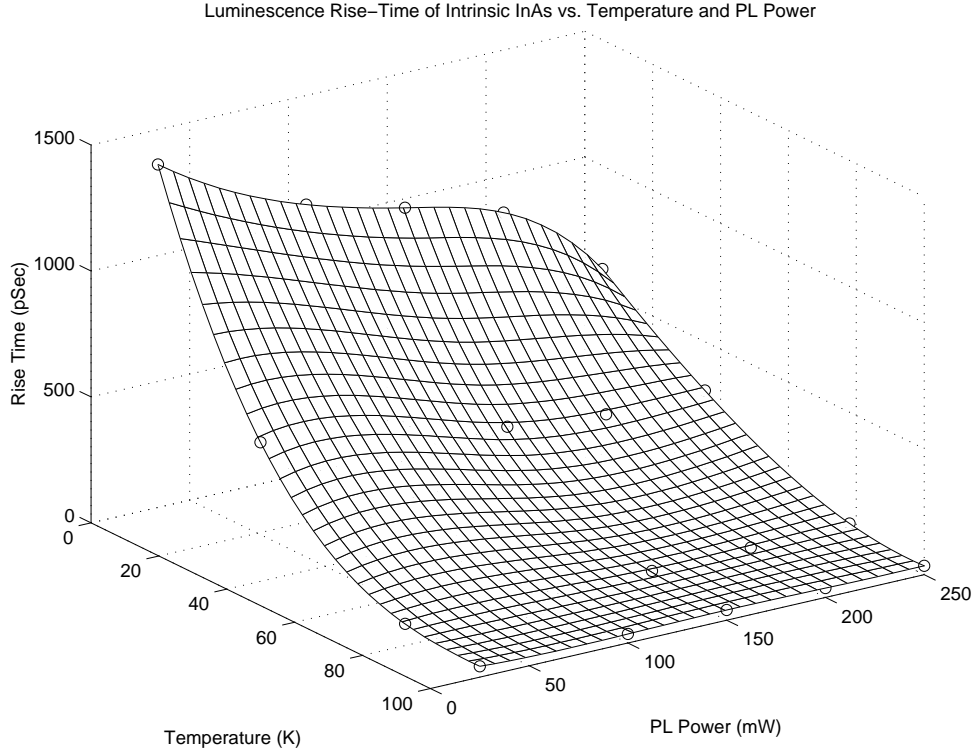


Figure 14 Bulk InAs rise time as a function of excitation power and temperature. Bicubic interpolation was used to smooth data. *See appendix A for code.*

in Fig.14. It can be seen that the luminescence rise time decreases both with increased temperature and increased excitation power.

The observed inverse relationship between the temperature and the carrier cooling time was explained previously in section 2.2. Lattice vibrations increase as the sample temperature increases, thus causing increased scattering and lower PL rise times. This also explains the decrease in rise time from the increased excitation power as well. At high excitation powers, carrier-carrier scattering initially dominates, but only until they reach a common temperature and as such, contribute little to carrier cooling in the lattice [17]. Since scattering from impurities is essentially constant, and InAs is not an alloy semiconductor, the only mechanism left is scattering from lattice vibrations. The inverse relationship between the excitation power and the luminescence rise time was also more pronounced at lower excitation powers for the evaluated range of temperatures. This is

of particular interest because it further strengthens the argument that excitation power is affecting the sample temperature. As a final premise to the argument, the monitored temperature of the thermocouple mounted to the cold finger was observed to raise by less than $2K$ at the combination of the lowest temperatures and the highest excitation powers. The flow of the liquid helium had to be increased at both the $5.2K$ and the $35.4K$ temperatures for excitation powers above $100mW$ in order to maintain the set temperature. This would indicate that a thermal gradient existed between the sample and the thermocouple since the samples were physically mounted approximately $1cm$ from the thermocouple. This would also indicate that while the monitored temperature did not appear to change at lower excitation powers, there would still be some heating due to the sample irradiance.

4.3 Type I Quantum Well Structure (94-099)

The next sample to be examined is the type I QW structure described in section 3.3. The results are tabulated in table 2 and can be seen in figures 15 and 16.

Table 2 Calculated type I quantum well structure rise time (psec) as a function of excitation power and temperature. Rise time is measured from the 10%-90% intensity points.

Power	100K	77K	35K	25K	5.8K
200mW	14.93	23.42	16.68	21.67	20.71
150mW	15.56	19.17	15.87	28.20	31.19
100mW	16.81	18.68	25.23	31.00	—
50mW	15.42	25.23	24.51	32.05	—
25mW	12.51	29.27	29.19	27.81	—

The first observation that can be clearly made is that the rise times are significantly less than those for the bulk InAs sample. The cause for this is most likely due to alloy scattering described in section 2.2. Since the wells have layers of $\text{InAs}_{0.9117}\text{Sb}_{0.0883}$, the random positioning of the Sb atoms in the InAs lattice cause a perturbation of the lattice potential resulting in a higher scattering rate in this material.

Besides the alloy scattering, the shorter rise times can also be attributed to the increased impurity content and the grain boundaries created when the well structure is grown. The dynamic range (shortest to longest) of the PL rise times at a given excitation power as temperature is increased (Fig.16) is significantly smaller than that of the intrinsic InAs. This provides further proof of scattering from processes other than those due to lattice vibration since that was the dominant process for the bulk InAs. The dynamic range of the PL rise times at a given temperature as excitation power is increased (Fig.15) is also smaller than that of the intrinsic InAs. It is this lack of dynamic range that ultimately makes analysis of this sample difficult. Any data variations introduced by the experiment would have less of an effect were this range greater which brings up a significant point.

In the course of this experiment, it was discovered that the experimentally measured values of the rise time could change significantly from day-to-day (or even occasionally from run-to-run) even though the alignment and calibration was performed daily. The

experiment was being used concurrently by Johnson [11] to measure carrier recombination dynamics and he reported similar problems with the data. The current consensus [10] is that the helitrans sample chamber is the most likely probable cause for this experimental error.

The helitrans sample chamber was mounted on a laboratory jack, enabling the sample to be positioned into the excitation beam. The jack adjustment was too coarse for minor adjustments and while every effort was made to keep from bumping it, any vibrations or motions could have affected the positioning of the sample. While this jack/sample chamber assembly was mounted directly to the floating optical bench, the cryogen transfer tube was connected between the dewar and the helitrans mounted to the top of the sample chamber. Thus, it is possible that the combined length of the helitrans and the transfer tube created a lever arm such that the weight of the transfer tube could have enabled the sample chamber to move. It was also discovered experimentally that the sample position was critical to the amount of PL signal collected for the QW samples, so any slight vibration could result in a significant change in the PL emitted power.

This having been stated, the lack of dynamic range and the variations in PL rise time for this sample made a three dimensional graph similar to that of Fig.14 difficult to interpret. As a result, the data for this sample was graphed individually as functions of excitation power (Fig.15) and temperature (Fig.16).

The best insight that analysis of these graphs can offer is general trends. At temperatures below 77K, Fig.15 shows that the PL rise time decreases with increasing excitation power. This result tends to support the weak indirect dependence of carrier density on rise time reported by Boggess [3]. Referring to Fig.16, there is a general trend of an inverse relationship between the PL rise and the sample temperature. This would again point to elevated sample temperatures with increased excitation power.

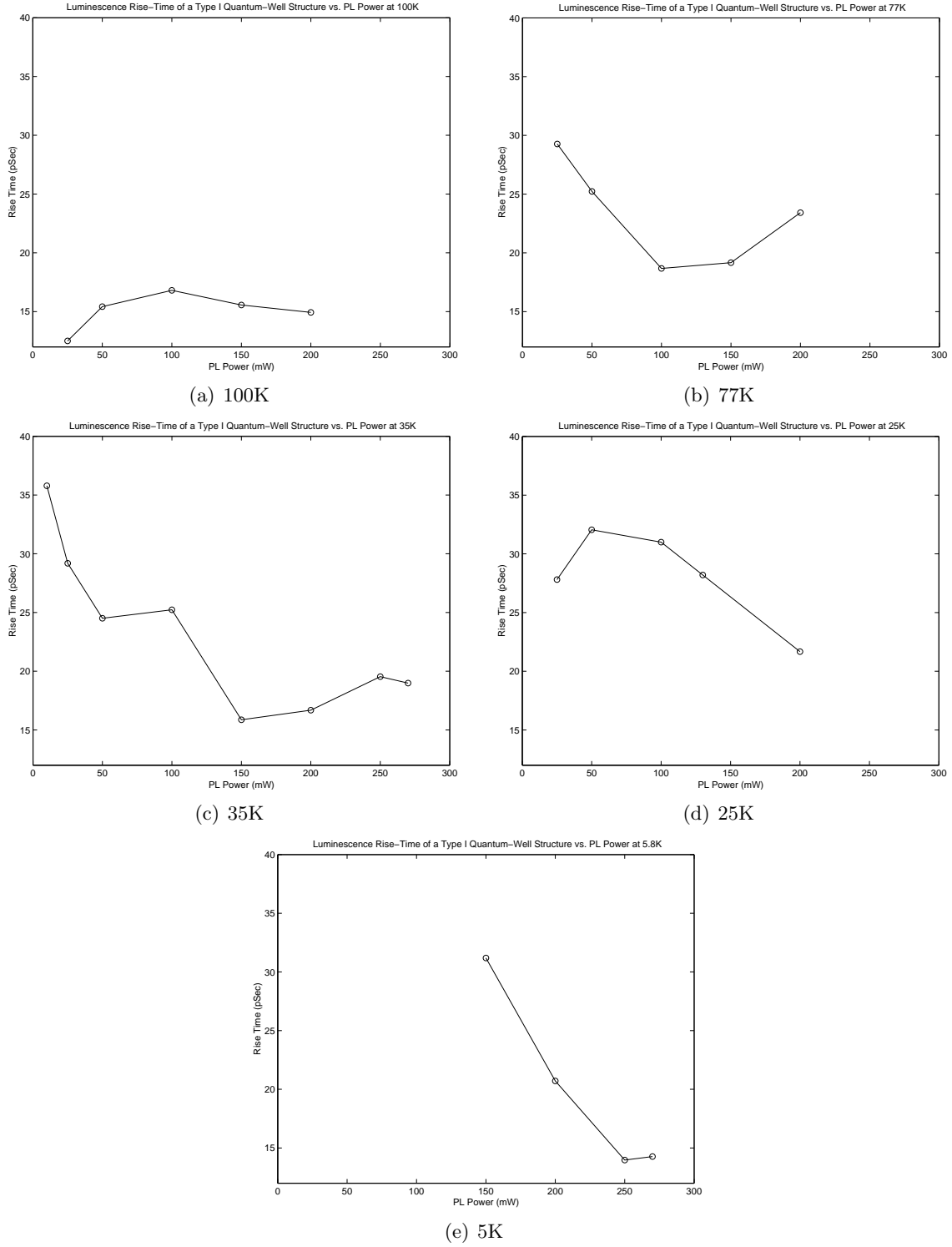


Figure 15 Luminescence rise time of a type I quantum well structure as a function of excitation power at various temperatures.

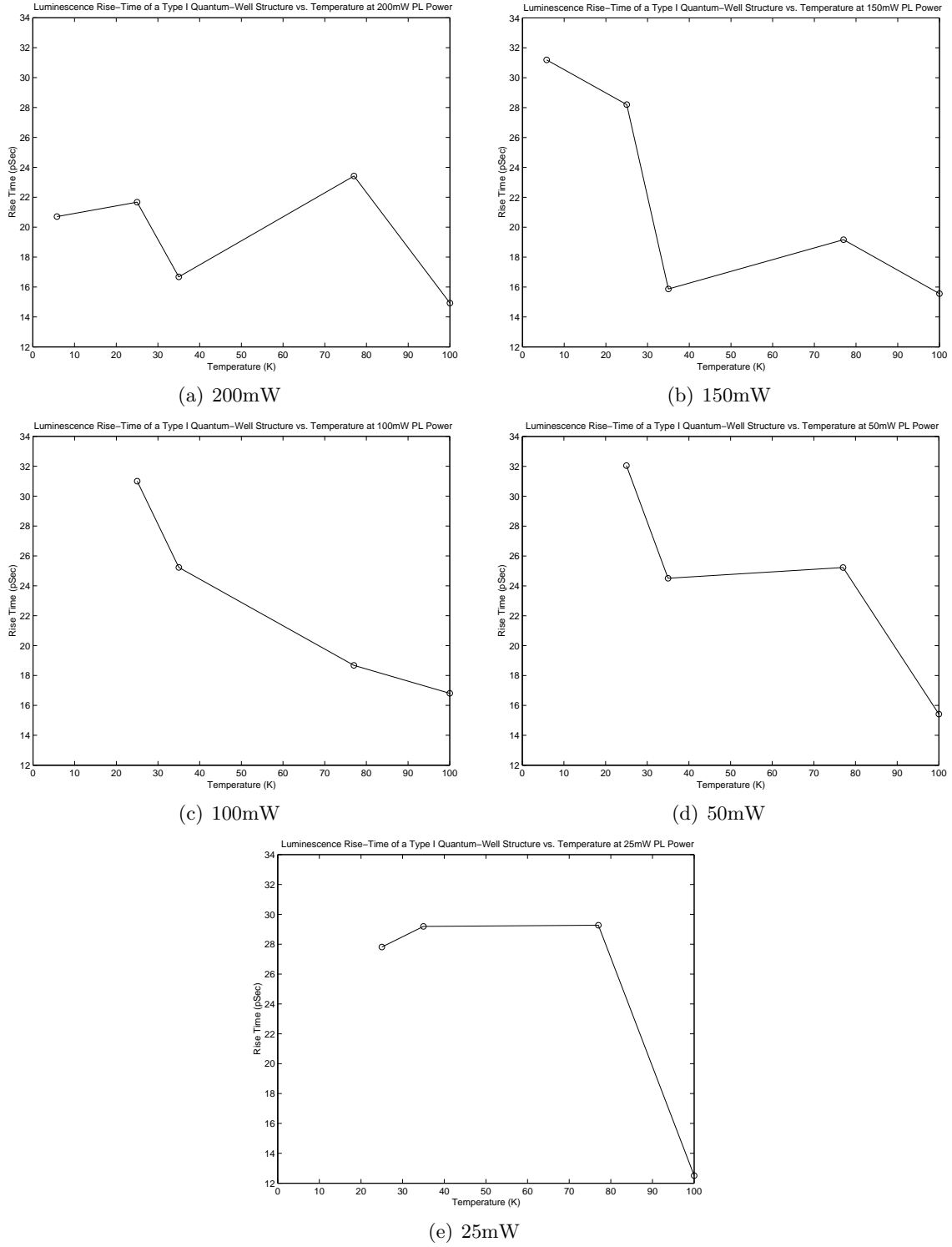


Figure 16 Luminescence rise time of a type I quantum well structure as a function of temperature at various excitation powers.

4.4 Type II Quantum Well Structure (200-91)

The last sample to be evaluated is the type II QW structure described in section 3.3. Analysis of its data proved inconclusive since variations of the measured rise time were again evident. The data results are compiled in table 3.

Table 3 Calculated type II quantum well structure rise time (psec) as a function of excitation power and temperature. Rise time is measured from the 10%-90% intensity points.

Power	100K	77.8K	38K
250mW	16.04	17.09	17.39
200mW	16.05	15.53	16.98
150mW	15.24	16.85	15.67
100mW	14.71	14.91	17.18
50mW	10.55	15.13	15.07
25mW	9.529	16.32	15.83
12.5mW	12.67	17.26	12.44
6.25mW	10.84	14.44	14.17

This sample was of particular interest because it had been previously evaluated for carrier cooling as a function of excitation power by Gorski [8]. While he only evaluated this sample at the single temperature of $77K$, he did evaluate it at four different excitation powers ($300mW$, $225mW$, $150mW$, and $75mW$). As stated previously, Gorski observed a direct dependence of carrier density on rise time as shown in table 4.

Table 4 Calculated rise time (in psec) for type II quantum well sample 200-91 as reported by Gorski [8]. Rise time is measured from the 10%-90% intensity points. Temperature is $77K$.

Power	Sample 200-91
300mW	16
225mW	12
150mW	5
75mW	4

While the data reported by Gorski is similar to that collected in this experiment at $300mW$, that is where the similarity ends. Gorski observed a rise time dynamic range of $4\times$ while this experiment resulted in fairly random data.

These results are unfortunate because this sample was also similar in construction to that examined by Boggess [3]. Because of this, it was hoped that by choosing a range of excitation powers that covered those used by both Gorski and Boggess, there would be a visible trend in the luminescence rise times that increased at both the low and high excitation powers. A minima between these points would indicate a critical excitation power where the hot phonon effect described in section 2.2.2 was just starting to be observed.

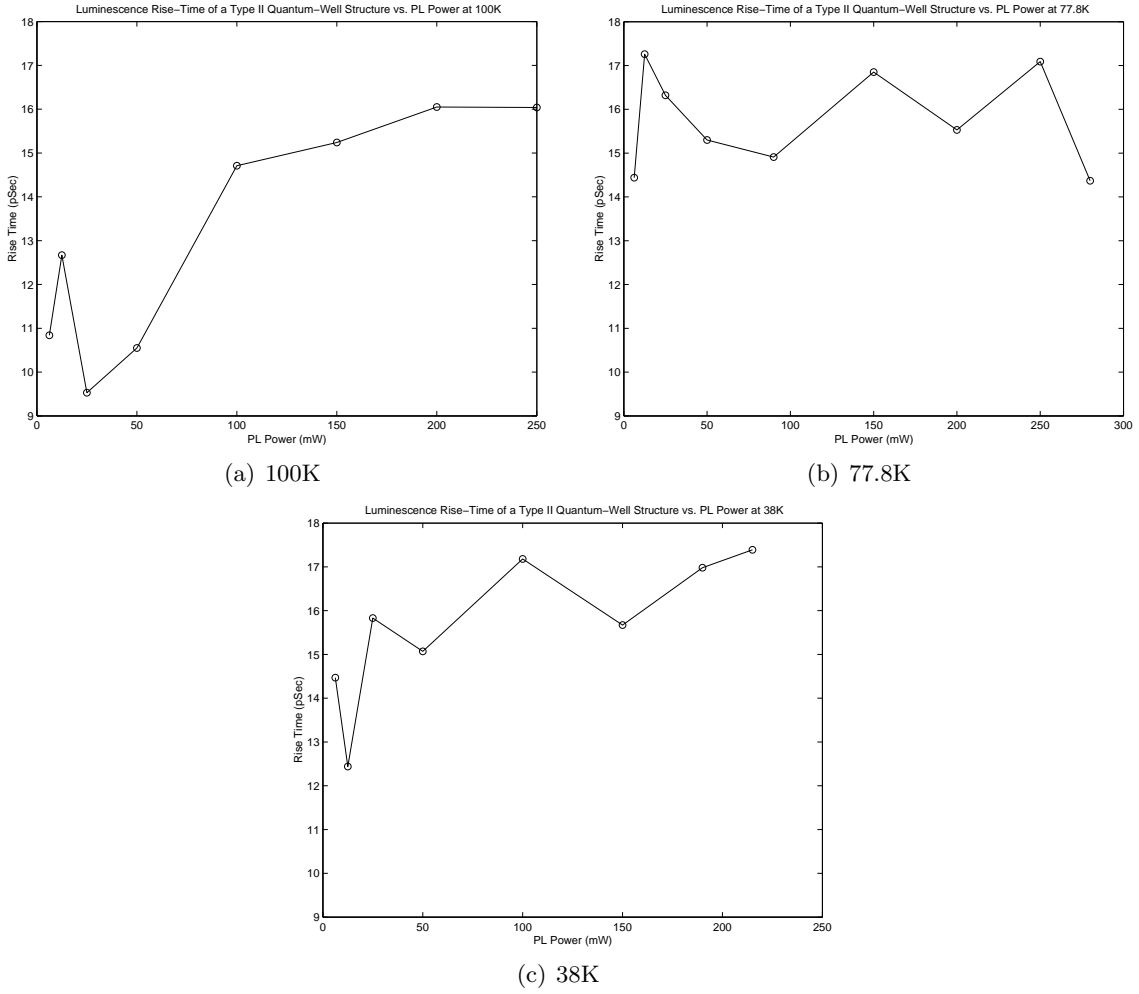


Figure 17 Luminescence rise time of a type II quantum well structure as a function of excitation power at various temperatures.

Data at 77.8K (Fig.17(b)) is random in nature and therefore, the results are inconclusive. The data at 100K and 38K, however, indicate a general trend of a direct correlation

between excitation power and luminescence rise time for excitation powers greater than $50mW$. This is in direct opposition to the previous cases of the bulk InAs and type I QW samples and is in line with the data previously reported on the same sample by Gorski [8]. Note that there is a slight peak below $50mW$ in the graphs at $100K$ and $77.8K$. This could be an indication that there is an inverse relationship between excitation power and luminescence rise time for very low excitation powers. If this were the case, it would prove to be the connection between the results reported by Boggess and those reported by Gorski. But, this connection is tenuous at best!

The excitation irradiance range reported by Boggess [3] was $1.5\mu W/cm^2 - 30\mu W/cm^2$. Gorski reported using a range of four excitation powers between $75mW$ to $300mW$ [8] which equates to an irradiance range of $15.5\mu W/cm^2 - 62.1\mu W/cm^2$. These irradiance calculations were based on the measured irradiance spot diameter of $90\mu m$ as reported by Johnson [11] and not the theoretical diffraction limited spot diameter of $39.1\mu m$ as reported by Gorski. The larger spot diameter was chosen because the components used in the experiment were the same as those used previously by Gorski. The range of excitation powers used for this sample was $6.25mW - 250mW$ which equates to an irradiance range of $1.29\mu W/cm^2 - 51.7\mu W/cm^2$. Again, this calculation is based on spot size of $90\mu m$ and a $76MHz$ PRR. Given this range, and assuming the results reported by both Boggess and Gorski are correct, the minima in luminescence rise time associated with the hot phonon effect threshold should be clearly observable. Unfortunately, this was not the case.

While the results in Fig.17 may hint at an increasing rise time at the lower powers, they are far from conclusive. The problem encountered with the low excitation powers was that the background signal level was too high and the exponential curve fit was not as accurate as those at higher excitation powers. An example of the data taken at an irradiance of $1.29\mu W/cm^2$ ($6.25mW$) was previously given in Fig.13. The variations in PL power emitted as a function of sample position was also a source of error.

Finally, referring to table 3, it is impossible to assess a general trend for the luminescence rise time as a function of sample temperature with any reliability.

4.5 Data and Analysis Conclusion

The data for the InAs clearly demonstrated that lattice vibrations due to sample temperature was the dominant scattering mechanism. The dynamic range of the rise times for this sample were exceptionally large allowing for a good analysis even with errors introduced through the experiment.

The data for the QW samples, while showing some general trends, was inconclusive. The additional scattering mechanisms of impurity and alloy scattering resulted in significantly shorter rise time dynamic ranges. Possible experimental errors were described along with the impact they would have on the data. Finally, the data for the type II QW structure hinted at a possible connection between the results reported by Boggess and Gorski, but was tenuous at best.

5. *Conclusions and Recommendations*

5.1 *Conclusions*

The ultimate goal of this thesis was twofold: the primary goal was to get the experiment up and running after a one-year hiatus, the secondary (and more significant) goal was to be able to reliably measure luminescence rise times of three MWIR samples. Closely related to this goal was the additional issue of trying to resolve the discrepancy between the results reported by Boggess [3] and those reported by Gorski [8]. In order to achieve this, the samples had to be evaluated at lower excitation powers than Gorski had used.

With respect to the primary goal, the results were successful. The experiment was finally operational after many hours of adjustments, alignments, and ultimately surmounting the significant learning curve associated with it. Experience and practice led to the measured data getting progressively better over time.

The secondary goal, while not necessarily providing the anticipated level of precision, was none-the-less achieved with some modicum of success. The results from the bulk InAs sample were the most pronounced and, as a result, the easiest to analyze and the most useful for future research. The results obtained from both the type I and type II quantum structures were less obvious although some general trend information was gleaned. With regards to trying to resolve the discrepancy mentioned above, there was still too much variation in the experimental results to arrive at a definitive answer. It is apparent that a significantly better signal-to-noise ratio of the upconverted signal will be necessary to achieve a higher level of precision.

5.2 *Recommendations*

One improvement that should be made to the experiment is to find a better method of mounting the sample chamber to the optical bench. The adjustment of the current laboratory jack was just too coarse to easily position the sample. There was a significant chance that it could move with the slightest vibration (as had been previously observed) and it is the most likely weak link in the experiment.

The KTA crystal should be replaced as it may have internal damage. Variations of up to an order of magnitude were observed in the background noise counts as the crystal was horizontally translated across its entire width. This would be due to internal scattering since the crystal surface was cleaned with acetone and had no observable scratches.

A “pulse picker” should be incorporated to the experiment to reduce the signal present at time t_0 . By using every other pulse from the Ti:sapphire laser, the PRR will be $38MHz$ resulting in a time between pulses of $26.3ns$. This will enable the luminescence from the QW samples to decay to the noise floor before the next excitation pulse arrives. This would ultimately lead to an increase of the signal-to-noise ratio of the luminescence, thereby increasing the accuracy of the experiment.

The samples used in this thesis were selected mainly because their structures were documented. However, they were physically small in size and their surfaces were less than optimum as they have been used many times by other researchers. New samples might help reduce the significant variations observed in collected PL power as a function of sample position. Also, variations of a sample type instead of different kinds of samples, e.g., type I QW structures with the same composition but different well widths, would be beneficial. This way, the carrier relaxation time can be compared in the context of how it is affected by varying well widths at a range of temperatures and excitation levels as discussed in section 2.3.

All of the runs for a given temperature should be performed as one uninterrupted set of runs in a day—varying the sample excitation power for each run. This will help reduce any variations due to alignment on a day-to-day basis.

The samples should be mounted as close to the thermocouple as possible so that the monitored temperature is as close to the sample temperature as possible. Also, a thermally conductive grease may prove to be a better mounting substance than the rubber cement that was used for this experiment. This may also help further reduce any thermal gradient between the thermocouple and the sample.

Finally, this could be a very useful experiment if the learning curve can be shortened. Using the alignment procedure outlined by Johnson [11], will be very useful in this respect.

While the alignment used by previous individuals [6, 13, 8] involved some amount of guess-work, careful measurements and documentation throughout this thesis process enabled the creation of a good working alignment procedure. Even so, there is still a certain amount of finesse necessary to achieve the best possible upconversion signal. The previous suggestion for new samples could help to minimize this, however.

Appendix A. MatLab Programs

A.1 MatLab Program for Fitting Exponential Curve to Rise Time Data

This program asks the user to input a two column, space-separated, data file of the form mmddyyr.dat where mm is the month, dd is the day, yy is the year, and run is a character a–z. The program then displays the data and asks the user to select a lower and upper limit upon which the exponential growth curve will be fit. The program then fits the data to an exponential growth curve of the form $U(1 - e^{(-t/\tau)})$ where U is a proportionality constant, t is the time, and τ is the time constant. The data is then plotted out along with the best calculated exponential curve fit. The expression for the exponential curve, the rise time, and the error standard deviation are also printed on the graph. Finally, the program determines if the best fit falls within the beginning and ending time constant values initially chosen—verifying that the program didn’t run out of range.

Clear all variables, close all figures, and clear the MatLab command window

```
clear all;  
close all;  
clc;
```

Enter the data file information

```
month = input('Enter the month > ','s');  
day = input('Enter the day > ','s');  
year = input('Enter the year > ','s');  
run = input('Enter the run > ','s');  
power = input('Enter the power > ','s');  
file = [month,day,year,run,'.DAT'];
```

Load data file and print data

```
data = load(file);  
time = data(:,1);  
counts = data(:,2);  
plot(time,counts,'*')
```

Enter the range of data on which to perform an exponential fit

```
lower = input('Enter the lower limit > ');  
upper = input('Enter the upper limit > ');
```

Reduce data file to the input range and close figure

```
time = time(lower:upper)-time(lower);  
counts = counts(lower:upper);  
counts = counts-counts(1);  
close(figure(gcf))
```

Initialize the squared error to the largest possible value

```
sqrerror_1 = sum(counts.^2)
```

Create an array of time constants and determine the squared error between the data and the exponential growth function at each time constant

```
for tau = time(end)/7:0.01:time(end)/3  
fit = [ones(size(time)) exp(-time/tau)];
```

Determine the proportionality constant

```
u = fit\counts;  
counts_temp = [ones(size(time)) exp(-time/tau)]*u;  
sqrerror = sum((counts-counts_temp).^2);
```

Check to see if the current squared error is less than the saved squared error and save the lesser of the two

```
if sqrerror<sqrerror_1  
sqrerror_1 = sqrerror;  
tau_result = tau;  
u_result = u;  
else  
break  
end  
end
```

Create an array for the best exponential curve fit and enter the current calculated values

```
trend = zeros(size(time,1),1);  
for n = 1:size(time,1),  
trend(n)=u_result(1)*(1-exp(-time(n)/tau_result));  
n=n+1;  
end
```

Determine the error standard deviation

```
RMS = sqrt(sum((trend-counts).^2)/size(counts,1));
```

Plot data with the calculated exponential curve

```
plot(time,counts,'.');
```

```
hold
plot(time,trend) t = 1e4;
```

Determine the rise time between 10% and 90% of U

```
full = u_result(1)*(1-exp(-1/tau_result*t));
c_low = full*0.10;
c_high = full*0.90;
t_low = -tau_result*log((u_result(1)-c_low)/u_result(1));
t_high = -tau_result*log((u_result(1)-c_high)/u_result(1));
rise_time = t_high-t_low;
```

Graph title—enter the sample and temperature before running

```
title(['Photon Counts vs. Time of an Intrinsic InAs Sample at 100K and ',num2str(power),'mW
Input Power'])
```

Print the equation for the exponential fit, the rise time, and the error standard deviation on the graph

```
words_1 = sprintf('Counts(t) = %0.4g*[1-exp(-%0.3g*t)]',u_result(1), 1/tau_result);
words_2 = sprintf('Rise Time = %2.4g picoseconds', rise_time);
words_3 = sprintf('Error Standard Deviation = %2.3g', RMS);
tmp1 = max(time)/4;
tmp2 = max(counts)/4;
text(tmp1, tmp2, words_1)
tmp1 = max(time)/4;
tmp2 = max(counts)/5;
text(tmp1, tmp2, words_2)
tmp1 = max(time)/4;
tmp2 = max(counts)/6.7;
text(tmp1, tmp2, words_3)
xlabel('Time (sec)')
ylabel('Photon Counts (30s ^{-1})')
```

Check to see if the calculated exponential curve is out of range of the initial guesses in the program

```
if time(end)/7 < tau_result
    sprintf('%s','good')
else
    sprintf('%s','bad')
end
if time(end)/3 > tau_result
    sprintf('%s','good')
else
    sprintf('%s','bad')
end
```

A.2 MatLab Program for Plotting a Three-Dimensional Curve of Luminescence Rise Time as a Function of Temperature and Excitation Power

This Program will plot a three dimensional bicubic interpolation of luminescence rise time as a function of temperature and excitation power. The user must create an array of temperatures, an array of excitation powers, and a matrix of measured rise times taken at each temperature/excitation power combination. The program then creates higher resolution temperature and excitation power arrays made up of 30 points between their respective low and high values. It then performs the interpolation and plots out the graph along with the original data points plotted as o's.

Clear all variables, close all figures, and clear the MatLab command window

```
clear all;  
close all;  
clc;
```

Create arrays of temperatures (x) and excitation powers (y) rise times (z)

```
x=[100 78 35.4 5.2];  
y=[250 200 150 100 25];
```

Create a matrix of rise times (z)

```
z=[35.35 58.74 306.5 590.1  
 36.85 53.08 302.0 904.7  
 40.47 50.59 343.4 1014  
 35.40 63.43 454.9 1117  
 42.58 66.47 507.1 1412];
```

Create a high resolution matrix between the minimum and maximum values of temperatures (xi) and the minimum and maximum values of power (yi)

```
xi=linspace(min(x),max(x),30);  
yi=linspace(min(y),max(y),30);  
[xxi,yyi]=meshgrid(xi,yi);
```

Perform a bicubic interpolation of the rise time values for the high resolution matrix

```
zzi=interp2(x,y,z,xxi,yyi,'cubic');
```

Plot the bicubic interpolation of the rise time as a function of the high resolution matrix and then plot the original data points as o's

```
mesh(xxi,yyi,zzz)
hold on
[xx,yy]=meshgrid(x,y);
plot3(xx,yy,z+0.1,'ok')
hold off
title('Luminescence Rise Time of Intrinsic InAs vs. Temperature and PL Power')
xlabel('Temperature (K)')
ylabel('PL Power (mW)')
zlabel('Rise Time (pSec)')
```

Bibliography

1. Agrawal, A. R. and N. K. Dutta. *Semiconductor Lasers* (2nd Edition). New York: ITP Van Nostrand Reinhold, 1993.
2. Bhattacharya, Pallab. *Semiconductor Optoelectronic Devices* (Second Edition). Prentice Hall, 1997.
3. Boggess, Thomas F., et al., "Ultrafast Optical Measurements of Carrier Dynamics in Antimonide-Based Quantum Wells." Thirteenth Annual Solid State and Diode Laser Technology Review, June 5-8 2000.
4. Boyd, R. W. *Nonlinear Optics*. San Diego, California: Academic Press, 1992.
5. Brown, Ronald F. *Solid State Physics: An Introduction for Scientists and Engineers*. San Luis Obispo, CA: El Corral Publications, 1999.
6. Cooley, W. T. *Measurement of Ultrafast Carrier Recombination Dynamics in Mid-Infrared Semiconductor Laser Material*. PhD dissertation, Air Force Institute of Technology, Wright-Patterson AFB, OH, December 1997.
7. Davis, L., et al. "Carrier Capture and Relaxation in Narrow Quantum Wells," *IEEE Journal of Quantum Electronics*, 30:2560 (1994).
8. Gorski, Steven M. *Carrier Dynamics in Mid-Infrared Quantum Well Lasers Using Time-Resolved Photoluminescence*. MS thesis, Air Force Institute of Technology, Wright-Patterson AFB, OH, March 2002.
9. Jang, D. J., et al. "Hot carrier dynamics in a (GaInSb/InAs)/GaInAlAsSb superlattice multiple quantum well measured with mid-wave infrared, subpicosecond photoluminescence upconversion," *Applied Physics Letters*, 70(9):1125-27 (March 1997).
10. Johnson, Peter M., 1stLt AFIT/ENP, "Personal Communication," February 2004.
11. Johnson, Peter M. *Deviation of Time-Resolved Luminescence Dynamics in MWIR Semiconductor Materials from Carrier Recombination Theory Predictions*. MS thesis, Air Force Institute of Technology, Wright-Patterson AFB, OH, March 2004.
12. Mahr, H. and M. D. Hirsch. "An Optical Up-Conversion Light Gate with Picosecond Resolution," *Optics Communications*, 13(2):96-99 (February 1975).
13. McKay, M.R. *Time-Resolved Photoluminescence of InAs/GaInSb Quantum Well Lasers*. MS thesis, Air Force Institute of Technology, Wright-Patterson AFB, OH, June 2001.
14. McKelvey, J. P. *Solid State Physics for Engineering and Materials Science*. Malabar Florida: Krieger Publishing Company, 1993.
15. Schepler, Kenneth. "Class Notes." OENG 660, Introduction to Nonlinear Optical Devices. Graduate School of Engineering and Management, Air Force Institute of Technology, Wright-Patterson AFB OH., Winter Quarter 2003.

16. Shah, Jagdeep. “Ultrafast Luminescence Spectroscopy Using Sum Frequency Generation,” *IEEE Journal of Quantum Electronics*, 24(2):276–288 (February 1988).
17. Shah, Jagdeep. *Ultrafast Spectroscopy of Semiconductors and Semiconductor Nanostructures*. Berlin: Springer, 1996.
18. Shah, Jagdeep, et al. “Subpicosecond luminescence spectroscopy using sum frequency generation,” *Appl. Phys. Lett.*, 50(19):1307–1309 (March 1987).
19. Website, Red Optronics, “<http://www.redoptronics.com/KTA-crystal.html>.” Electronic Communication, April 2004.
20. Yang, C. H., et al. “Hot electron Relaxation in GaAs Quantum Wells,” *Physical Review Letters*, 55(21):2359–2361 (November 1985).
21. Yariv, A. and P. Yeh. *Optical Waves in Crystals: Propagation and Control of Laser Radiation*, Hoboken, New Jersey. John Wiley & Sons, Inc., 2003.

REPORT DOCUMENTATION PAGE					Form Approved OMB No. 074-0188	
<p>The public reporting burden for this collection of information is estimated to average 1 hour per response, including the time for reviewing instructions, searching existing data sources, gathering and maintaining the data needed, and completing and reviewing the collection of information. Send comments regarding this burden estimate or any other aspect of the collection of information, including suggestions for reducing this burden to Department of Defense, Washington Headquarters Services, Directorate for Information Operations and Reports (0704-0188), 1215 Jefferson Davis Highway, Suite 1204, Arlington, VA 22202-4302. Respondents should be aware that notwithstanding any other provision of law, no person shall be subject to a penalty for failing to comply with a collection of information if it does not display a currently valid OMB control number.</p> <p>PLEASE DO NOT RETURN YOUR FORM TO THE ABOVE ADDRESS.</p>						
1. REPORT DATE (DD-MM-YYYY) June 2004		2. REPORT TYPE Master's Thesis		3. DATES COVERED (From – To) Sep 2003 – Jun 2004		
4. TITLE AND SUBTITLE Using Time-Resolved Photoluminescence to Measure the Excitation and Temperature Dependence of Carrier Relaxation in Mid-Wave Infrared Semiconductors				5a. CONTRACT NUMBER		
				5b. GRANT NUMBER		
				5c. PROGRAM ELEMENT NUMBER		
6. AUTHOR(S) Cumblidge, Kevin, Civ.				5d. PROJECT NUMBER 04-156		
				5e. TASK NUMBER		
				5f. WORK UNIT NUMBER		
7. PERFORMING ORGANIZATION NAMES(S) AND ADDRESS(S) Air Force Institute of Technology Graduate School of Engineering and Management (AFIT/EN) 2950 P Street, Building 641 WPAFB OH 45433-7765				8. PERFORMING ORGANIZATION REPORT NUMBER AFIT/GAP/ENP/04-02		
9. SPONSORING/MONITORING AGENCY NAME(S) AND ADDRESS(ES) Air Force Office Of Scientific Research 801 North Randolph Street Arlington, VA 22203-1977				10. SPONSOR/MONITOR'S ACRONYM(S) AFOSR/MOA		
				11. SPONSOR/MONITOR'S REPORT NUMBER(S)		
12. DISTRIBUTION/AVAILABILITY STATEMENT APPROVED FOR PUBLIC RELEASE; DISTRIBUTION UNLIMITED.						
13. SUPPLEMENTARY NOTES						
14. ABSTRACT Research in the field of mid-wave infrared (MWIR) semiconductor photonic devices has led to applications in a variety of disciplines including atmospheric monitoring, optical communications, non-invasive glucose testing for diabetics, and infrared (IR) countermeasures. One of the limiting factors for improving the modulation rates of MWIR devices is the carrier relaxation time. This is the time required for energetic carriers to cool to the edge of their respective bands in a bulk semiconductor material, or to the bottom of a well through inter- and intra-sub-band scattering in a quantum well (QW) structure. From these lower energy states, they can then recombine radiatively in photonic devices. This investigation utilized the nonlinear optical technique of frequency upconversion to perform time-resolved luminescence spectroscopy on epitaxial bulk InAs, InAsSb/InAlAsSb type I QW structure, and InAs/GaInSb type II QW samples to calculate carrier relaxation times in each as a function of excitation irradiance and sample temperature.						
15. SUBJECT TERMS Time Resolved Luminescence Spectroscopy, MIWR semiconductors, Carrier Relaxation, Carrier Cooling						
16. SECURITY CLASSIFICATION OF:			17. LIMITATION OF ABSTRACT UU	18. NUMBER OF PAGES 62	19a. NAME OF RESPONSIBLE PERSON MICHAEL A. MARCINIAK AFIT/ENP	
REPORT U	ABSTRACT U	c. THIS PAGE U			19b. TELEPHONE NUMBER (Include area code) (937) 255-3636, ext4529; e-mail: Michael.Marciniak@afit.edu	